ARC Alliance

ARC Geophysical Research

GR Geophysical Research

Investigating the Interplay of Permeability and Roughness on Patchy Vegetated Hillslopes *in Silico*

Octavia Crompton *[1], Gabriel Katul[2], and Sally Thompson [3]

[1]USDA-ARS Hydrology and Remote Sensing Laboratory

[2]Duke University

[3]University of Western Australia

Abstract

On hillslopes with patchy vegetation cover, vegetation is a significant factor controlling surface hydraulic and hydrological properties. Soil permeability is often greater within vegetated areas than in surrounding bare soil areas, leading to the redistribution of rainfall from bare, runoff-generating areas to permeable, vegetated areas. While many studies have examined the hydrological consequences of permeability contrasts, the hydrodynamic effects of greater surface roughness in vegetated patches compared to bare areas remain under-investigated. The role of roughness is not obvious: greater roughness in vegetated patches provides greater resistance to flow, slowing water movement and thus extending the time frame over which infiltration can occur. However, greater roughness may also cause partial blocking and flow diversion, reducing the volume of water traversing vegetated areas, a mechanism that could reduce rainfall redistribution to these sites.

To differentiate the roles of spatially-varying roughness and permeability on rainfall redistribution, the two-dimensional Saint Venant Equations are employed to model the hydrologic outcomes of permeability and roughness contrasts under varying rainfall intensities. The simulations consider the dynamically interesting case of an idealized vegetated patch surrounded by runoff-generating unvegetated areas. The model results indicate that greater resistance causes flow diversion around vegetation. However, vegetative resistance only reduces rainfall redistributed to the vegetation under the specific conditions of low rainfall intensity and high soil permeability. Otherwise, prolonged ponding during the recession period, due to greater vegetative resistance, creates additional time for infiltration, compensating for increased flow diversion around the vegetation.

Keywords: Source-Sink Dynamics, Surface Roughness, Vegetation Spatial Pattern, Hydrological Connectivity

*Corresponding Author

E-mail addresses: octavia.crompton@gmail.com

1 Introduction

Drylands – water-limited regions with arid, semiarid, and dry subhumid climates – receive limited rainfall that is generally insufficient to sustain continuous plant cover [33, 46]. In these regions, vegetation often grows in patches interspersed with areas of bare soil [43, 45]. Soil permeability is typically higher under vegetation cover than in bare soil areas, which form low-permeability surface crusts [3, 5, 22]. Higher soil permeability in vegetated patches promotes 'run-on' behavior: sporadic, but often intense, rainfall produces infiltration excess runoff [41, 42], which flows downslope or to sites with high permeability, typically vegetated patches where protected and biologically disturbed soils enhance permeability [2, 32]. This redistribution of rainfall runoff from bare soil to vegetated patches supplements plant water and nutrient resources, sustaining vegetation in regions where annual rainfall alone would be insufficient [22, 40, 51].

In these environments, storm-scale hydrological processes are dominated by infiltration-excess overland flow infiltration-excess overland flow dominates storm-scale hydrological processes, with runoff generated when rainfall intensity exceeds the local infiltration capacity [3, 22]. Vegetation typically grows in patches interspersed with crusted, bare soil areas, and this spatial heterogeneity in surface and soil hydraulic properties strongly influences overland flow [43, 45].

More tortuous flow paths that bypass vegetation can also form, for example, where plants grow on mounds that form as a result of differential interrill erosion, splash erosion and sedimentation between plant patches and bare soil areas [7, 37, 60]. Microtopographic mounds may route flow around the vegetation for shallow flows, such that enhanced permeability under vegetation only promotes infiltration if flows are sufficiently deep to inundate the microtopography [50, 61]. In the absence of microtopography, greater surface roughness – and thus greater resistance to flow – in vegetated sites may have a secondary rerouting effect, similar to that of microtopography [14]. Whether such flow diversion enhances or inhibits run-on infiltration in vegetated areas remains an open question and frames the scope here.

On the one hand, increasing resistance to overland flow reduces the flow velocity and increases the residence time of runoff traversing vegetated patches. Thus, greater surface roughness could increase the time opportunity for runoff to infiltrate into vegetated patches, most importantly during the rising and recession periods of storms and other transient periods such as breaks in rain [24–26]. Vegetation roughness would thus amplify the influence of permeability on runoff redistribution, enhancing the redistribution of runoff due to permeability differences between vegetation and bare soil. On the other hand, greater surface roughness may obstruct and divert runoff from the vegetation [58], increasing the tortuosity of flow paths and reducing the transport of water and other resources to vegetated areas.

Thus, greater soil permeability in vegetated areas creates local depth gradients that drive the flow towards the vegetation [56], whereas greater roughness may both slow flow within and divert runoff around it. In empirical studies, distinguishing these different influences is challenging because soil permeability and surface roughness are spatially correlated [but see 58]. This complexity makes the problem well-suited to physics-based modeling approaches that

doi: https://10.5149/ARC-GR.1384

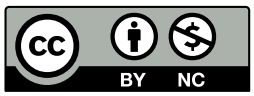

allow for independent exploration of permeability-roughness interactions under varying landscape, vegetation, and rainfall characteristics, and the implications for the spatial distribution of infiltrated water.

Here, the Saint Venant Equations (SVE) coupled to an infiltration model are used to represent rainfall-runoff and infiltration for discrete storm events on an idealized planar hillslope. This hillslope consists of bare soil surrounding a circular vegetation patch. Three scenarios with contrasting vegetation-bare soil properties are modeled: (i) permeability-only, in which soil permeability is greater in the vegetation relative to bare soil, but roughness properties are the same, (ii) roughness-only, in which surface roughness is greater in the vegetation, but soil permeability is constant between bare and vegetated areas, and (iii) combined, in which both permeability and roughness differ between bare soil and vegetation. Passive tracers advected by the bulk flow are used to quantify runoff diversion around the patch, while cumulative infiltration is computed for every point in the domain. The flow diversion and infiltration behaviors are then compared between scenarios, for varying storm and landscape conditions, to assess the effects of roughness in vegetated areas on run-on infiltration in the vegetated patch.

2 Methods

Section 2.1 reviews the SVE model, including the parameterization of flow resistance and infiltration. Section 2.2 details how these parameterizations are modified for the roughness-only and permeability-only scenarios, and Section 2.3 describes the particle tracing to identify flow paths. Other aspects of the simulation domain are presented in Section 2.4, including the rainfall and hillslope characteristics.

2.1 The Saint Venant Equations

Sheet flow during storm events typically results in shallow flows (<5 cm), which can locally vary in depth and depth-averaged velocity, as water passes over surfaces of variable permeability and roughness. Such shallow, unsteady and heterogeneous flows are commonly represented by the Saint Venant Equations (SVE) or 'shallow water equations' [8], which in two dimensions and for small slope angles take the form:

$$\frac{\partial h}{\partial t} + \frac{\partial (Uh)}{\partial x} + \frac{\partial (Vh)}{\partial y} = p - i \tag{1}$$

$$\frac{\partial U}{\partial t} + U\frac{\partial U}{\partial x} + V\frac{\partial U}{\partial y} + g\frac{\partial h}{\partial x} + g(S_{fx} - S_x) = 0 \tag{2}$$

$$\frac{\partial V}{\partial t} + U\frac{\partial V}{\partial x} + V\frac{\partial V}{\partial y} + g\frac{\partial h}{\partial y} + g(S_{fy} - S_y) = 0 \tag{3}$$

where i is the infiltration rate that is set by the smaller value of the infiltration capacity and rainfall intensity p, U, V denote the depth-averaged flow velocities in the x (longitudinal) and y-directions (lateral), respectively; h is the depth of flow; S_x and S_y are the bed-slope in the x and y directions; t is time; and g represents gravitational acceleration. The terms S_{fx} and S_{fy} are the x- and y- components of the friction slope (or energy gradient), which represent the effect of bed and other shear stresses on retarding the flow. The SVE do not form a closed system of equations, so a 'closure' model in the form of a resistance formulation must be specified to represent the net effects of bed and other shear stresses (e.g., presence of obstructions) on the friction slope. Flow resistance depends on the flow state commonly represented by bulk flow properties such as the Reynolds number, the Froude number, surface

roughness, or the velocity and water depth. While the prediction of overland flow resistance remains an ongoing challenge [36, 53], the model results are not anticipated to depend on the choice of resistance formulation (see, for example, the studies of Mügler et al. [39], Cea et al. [9], and Crompton et al. [13], demonstrating that multiple resistance formulations can produce acceptable agreement with runoff measurements through calibration). Thus, we adopt an approach that allows for a contrast in roughness between bare soil and vegetated areas by accounting for resistance from the bed and vegetation elements. This formulation begins with a quadratic drag-law:

$$\begin{aligned} S_{f,x} &= R_h U|U| \\ S_{f,y} &= R_h V|U| \end{aligned} \tag{4}$$

where $|U| = \sqrt{U^2 + V^2}$ is the flow speed and R_h is a resistance factor determined by the vegetation and soil properties. This formulation for $S_{f,x}$ and $S_{f,y}$ ensures that flow resistance is always acting against the direction of flow. For very shallow flows typical of storm runoff, bed resistance is likely to be significant, in addition to canopy resistance. To accommodate both surface cover types in a single resistance formulation, the approach described by James et al. [referred to as the James Formulation hereafter, 30] is employed. This approach is grounded in empirical runoff studies and extensive work characterizing resistance to flow through vegetation [see 54, and references therein]:

$$R_h = \frac{1}{(1-\phi_V)gh}\left(\frac{f}{8} + \frac{1}{2}C_d h D N\right), \tag{5}$$

where f is the Darcy-Weisbach friction factor for the soil surface, D is the stem diameter, ϕ_V is the stem density (i.e., the volume fraction occupied by the vegetation), $N = 4\phi_V(\pi D^2)^{-1}$ is the stem count per unit area (i.e., stems m$^-2$), and C_d is a vegetation drag coefficient, which depends on the vegetation characteristics and the flow speed $|U|$. To represent dryland grasses or shrubs, a 'cylinder array' formulation for the drag coefficient is used [10]. This formulation accommodates sheltering and blockage effects on the drag coefficient of the cylinder array. Details of the C_d formulation used here are presented in supporting information (SI) Text S1. Throughout this modeling study, the roughness of the vegetation is adjusted by altering the stem density ϕ_V. Anticipating low bulk Reynolds numbers ($Re = Uh/\nu < 500$, ν is kinematic viscosity) for the simulated rainfall intensity and hillslope dimensions (see Section 2.4), f is given by a modified laminar formulation that is identical for bare soil and vegetation (also described in SI Text S1). To summarize, both stem drag and surface friction can be significant in vegetated areas, with stem drag most important for deeper flows and ground friction most important in shallower conditions. Bare soil is characterized by $\phi_V = 0$, so that $R_h = f/(8gh)$, which is the conventional form used when the water depth exceeds the mean surface protrusion height into the flow.

While the James formulation is used throughout, other roughness schemes are commonly employed to model runoff, such as Manning's equation and its associated roughness [28, 31]. To test the sensitivity of the modeling results to the choice of resistance formulation, supplementary simulations were run with Manning's equation ($S_f = nU^2h^{-4/3}$, where n is the Manning coefficient), with $n_b = 0.03$ for bare soil areas and n_V ranging from 0.2 - 0.8 for vegetation [11]. The results, presented in Text S2, indicate qualitatively similar results to those obtained with the James formulation. For this reason the outcomes from the James formulation are only presented.

Infiltration capacities in the model, like resistance, are determined by whether the surface cover is bare or vegetated. This binary treatment of the landscape is similar to previous modeling efforts, field and remote sensing studies [e.g., 1, 12, 29, 38, 47]. To simplify the

problem, the infiltration capacity is assumed to be constant and equal to the local saturated hydraulic conductivity K_s, with K_V and K_B distinguishing vegetation and bare soil areas. The infiltration rate is then computed as: $i = \min(K_s, p + h/\Delta t)$, where h is the local surface water depth and Δt is the model timestep. This choice may underestimate the true infiltration capacity as it ignores sorptive effects, which may be large for initially dry soils (but are small for initially wet soils). It allows, however, for treatment of permeability contrast using a single parameter K_s, like roughness, to be dictated solely by whether the surface is bare or vegetated.

In all simulations, the flow is assumed to be subcritical at all times and locations, such that the Froude number $Fr = U(gh)^{-1/2}$ remains below unity. This assumption was confirmed post-hoc by examination of the simulation results. While the validity of the SVE makes no a priori assumption about Fr, the $S_{f,x}$ and $S_{f,y}$ formulations here do not accommodate energy losses due to hydraulic jumps (HJs) at super-critical to sub-critical flow transitions. HJs occur when the flow is forced to transition from a fast super-critical ($Fr > 1$) state to a slower, sub-critical ($Fr < 1$) state, dissipating excess kinetic energy by creating intense turbulence zones in the pile-up region. Since HJs are not captured by the aforementioned $S_{f,x}$ and $S_{f,y}$ formulations used here, ensuring that $Fr < 1$ for all locations and time instances ensures that no HJs are encountered – i.e., the model is self-consistent. While this assumption is appropriate for the modeled domain, the occurrence of hydraulic jumps depends on a forced transition from supercritical to subcritical flow [11]. In real-world rainfall-runoff settings, it remains understudied and likely depends on local surface conditions (e.g. topography and local obstructions by roughness elements) and flow conditions (zones of elevated velocities and shallow depths leading to supercritical flows).

The SVE model is solved using FullSWOF-2D [19], an open-source two-dimensional Saint Venant Equation (SVE) model that is capable of representing transient and spatially-heterogeneous surface properties. FullSWOF-2D has been validated on a library of analytic solutions to the SVE [18] and real rainfall events [55]. When trialed against 112 rainfall experiments [44], the median Nash-Sutcliffe Efficiency (NSE) for reproducing the hydrographs was 0.95, SD = 0.13 (see SI Figures S1 showing sample calibration results) [16, 17]. Thus, the numerical simulations of the SVE using FullSWOF-2D are supported by this large body of relevant prior lab and field experiments.

2.2 Roughness-Only and Permeability-Only Scenarios

Three broad model scenarios were run to isolate surface roughness from permeability effects. In the combined-effects simulations, both roughness and permeability differed between bare soil and vegetation, as above. In the permeability-only simulations, soil permeability was greater in the vegetation ($K_V > K_B$), while surface roughness was uniform and given by the bare soil parameterization ($\phi_V = 0$ and $R_h = f/(8gh)$). In the roughness-only simulations, surface roughness was greater in the vegetation, while soil permeability was uniform and equal to K_B. To separate the effects of roughness from permeability, the analysis then compares hydrologic outcomes between the three scenarios for common variables (i.e., paired simulations in which all variables are identical except for the roughness or permeability).

2.3 Lagrangian Tracers

For each SVE simulation, 1000 tracers were released at the domain's upslope boundary, with initial y-positions uniformly spaced between the lateral boundaries. The tracers were released at random times between $t = 0$ and the rain duration t_R, such that the tracer trajectories reflect flow conditions over the storm duration. The trajectory of each tracer was determined assuming only advection by the computed 2-dimensional velocity vector. At each timestep

Table 1: Parameters used in the SVE model simulations. Where multiple entries are listed, the cases were run factorially to explore all parameter combinations. Note that the listed K_V values apply only to the combined-effects and permeability-only scenarios, and the ϕ_V and D values apply to the combined-effects and roughness-only scenarios (see Section 2.2).

Variable	Symbol	Values
Boundary conditions		
Slope gradient (%)	S_o	1%
Domain size	W_x, W_y	40 m × 30 m
Patch radius	r	5 m
Within-patch stem density (volume fraction)	ϕ_V	0.1, 0.2, 0.3
Stem diameter	D	5 mm
Saturated hydraulic conductivity (vegetation)	K_V	5, 15 cm/hr
Saturated hydraulic conductivity (bare soil)	K_B	0.5 cm/hr
Storm cases		
Rainfall intensity	p	2, 4, 6, 8, 10 cm/hr
Storm duration	t_R	10 minutes

dt, a given tracer infiltrated with probability $i \cdot dt/(h' + p)$, where i is the local infiltration rate (i.e., K_V or K_B when ponding occurs) and h' is the flow depth at the tracer's location. The tracer computations were separately validated by comparing the runoff coefficient in the SVE model to the fraction of tracers that exit the hillslope as runoff.

2.4 Simulation Domain

To simplify interpretation of the results, the model domain consisted of a circular vegetation patch of radius $r = 5$ m, situated in an otherwise uniform bare soil domain on a planar hillslope of length $W_x = 40$ m and width $W_y = 30$ m (see Figure 1). This hillslope was sufficiently wide for the flow to be 1-dimensional adjacent to the lateral boundaries ($V/U < 1e^{-4}$). Surface roughness in bare soil areas was held constant across all simulations, and was varied in the vegetation patch by adjusting the stem density ϕ_V, while holding the stem diameter D constant at 5 mm. As outlined in the supporting information (Equations 3-4) adjusting either ϕ_V or D produces equivalent effects on S_f and concomitant solutions to the SVE.

The SVE model was used to simulate rainfall runoff for a broad range of storm and soil characteristics, summarized in Table 1, varying the boundary conditions (i.e., surface roughness and soil permeability) and rainfall intensity. The saturated hydraulic conductivities in the vegetation patch, $K_V = 2, 5, 10, 15$ cm/hr, and surrounding bare soil, $K_B = 0.5$ cm/hr, are representative values selected from field studies [e.g., 22, 59]. The rainfall intensity ranges from $p = 2$ to 10 cm/hr, spanning resource-shedding cases ($p > K_V$), where the patch generates runoff during the storm, to resource-capturing cases ($p < K_V$), where the patch receives run-on from the upslope bare soil area during the storm. In both cases, runoff from upslope contributes to patch infiltration after the storm.

For visual clarity, results pertaining only to $K_V = 2$ and 10 cm/hr are shown in the main text figures, and equivalent figures that include all K_V are presented in the supporting information. In total, 60 simulations were run, comprising 30 combined-effects cases, 15 permeability-only cases, and 15 roughness-only cases.

2.5 Scenario Assessment Metrics

Table 2 summarizes the assessment metrics used in the study. Firstly, the maximum flow depth $h(t_R)$ is examined to visualize how spatially varying roughness and permeability influence the flow. Greater roughness in the vegetation promotes deeper flows, whereas greater permeability lowers the flow depth as water is lost to infiltration. Because the rainfall intensity is constant, the maximum flow depth occurs at the storm end (time $t_R = 10$ min).

While the maximum flow depth provides a snapshot of the flow field at time t_R, the cumulative infiltration after the storm ends provides an integrative measure of the water partitioning on the landscape, computed as:

$$I(x, y) = \int_{t=0}^{\infty} i(x, y)dt, \tag{6}$$

where i is the instantaneous rate of infiltration. The cumulative infiltration can be directly interpreted as measuring the duration that surface water was present at a given point in the landscape, since the duration of surface ponding and infiltration capacity jointly control the infiltration at a point.

Next, we consider the patch infiltration depth I_V, which is the spatial average of the cumulative infiltration in the vegetation patch and is given by:

$$I_V = \frac{1}{\pi r^2} \int_V I(x, y)dA \tag{7}$$

where $\int_V$ indicates integration over the patch area. Since I_V increases with increasing incident rainfall, we also examine the patch infiltration fraction IF_V, which is defined as the cumulative patch infiltration normalized by rainfall depth $d_R = pt_R$:

$$IF_V = \frac{I_V}{d_R}. \tag{8}$$

In resource-capturing cases ($p < K_V$), run-on is directed towards the patch both during and after the rainfall, and net run-on to the vegetation is expected ($IF_V > 1$). In resource-shedding cases ($p > K_V$), the patch generates runoff during rainfall but may also capture runoff from upslope bare soil areas during the recession period. Thus, net run-on or net runoff from the patch are both possible. Whether the patch is a net runoff source ($IF_V < 1$) or sink ($IF_V > 1$) depends on how much runoff the patch generates during the rainfall compared to how much it captures during the recession period. These outcomes, in turn, depend on the infiltration capacity of the patch and the duration of surface ponding after the rainfall ends.

To identify how different processes lead to these contrasting outcomes, we separately assessed infiltration occurring during the rainfall and recession periods. The factors that influence infiltration – and the role of vegetative resistance – vary across rainfall and recession periods, and between resource-shedding and resource-capturing regimes. Table 3 summarizes the controls on patch infiltration for each combination of (i) rainfall and recession periods, and (ii) resource-shedding and resource-conserving cases.

The cumulative infiltration during the rainfall is defined as:

$$I^{rain}(x, y) = \int_{t=0}^{t_R} i(x, y)dt, \tag{9}$$

and similarly for the recession period:

$$I^{rec}(x, y) = \int_{t=t_R}^{\infty} i(x, y)dt. \tag{10}$$

Table 2: Summary of the assessment metrics. The 'Distributed' column indicates whether each variable is computed across the spatial domain (Yes) or summarized over the vegetation patch or domain as a whole (No).

Variable	Description	Units	Distributed
Scenario assessment metrics			
$h(t_R)$	Maximum flow depth	m	Yes
I	Infiltration depth	m	Yes
I^{rain}	Infiltration depth during the rainfall period	m	Yes
I^{rec}	Infiltration depth during the recession period	m	Yes
I_V	Patch infiltration depth	m	No
IF_V	Patch infiltration fraction ($IF_V = I_V/d_R$)		No
${I_V}^{rain}$, ${I_V}^{rec}$	I_V during the rainfall and recession periods	m	No
${IF_V}^{rain}$, ${IF_V}^{rec}$	IF_V during the rainfall and recession periods		No
ξ	Flow diversion, defined as the fraction of the tracers initialised upslope of the vegetation patch that bypass it		No
$F_{pond}(t)$	Inundated fraction of the patch as a function of time		No
$q_L(t)$	Hillslope hydrograph, defined as the runoff flux across the downslope boundary as a function of time	cm/hr	No
Scenario inter-comparison metrics			
ΔIF_V	Difference in IF_V between paired permeability-only and combined-effects simulations		No
$\Delta\xi$	Difference in ξ between paired roughness-only and combined-effects simulations		No

Equivalently, $I^{rec}(x, y) = I - I^{rain}(x, y)$.

The patch infiltration depths over the rainfall and recession periods, ${I_V}^{rain}$ and ${I_V}^{rec}$, are defined analogously to I_V (Equation 7), and the patch infiltration fractions, ${IF_V}^{rain}$ and ${IF_V}^{rec}$, are defined analogously to IF_V (Equation 8, normalizing infiltration in each period by the rainfall total). Thus, by definition, ${IF_V}^{rain} + {IF_V}^{rec} = IF_V$ in both cases.

If the rainfall intensity exceeds the patch infiltration capacity ($p > K_V$), the patch will generate runoff during the rainfall period (${IF_V}^{rain} < 1$), while the converse (${IF_V}^{rain} > 1$) should occur if $p < K_V$. Since no runoff is generated after the rain stops, ${IF_V}^{rec} \leq 1$.

The hillslope hydrograph, $q_L(t)$, is defined as the runoff flux across the downslope boundary as a function of time, providing an integrated measure of the hillslope's runoff response to rainfall. To characterize the duration of ponding in the patch, we computed the patch inundated fraction, $F_{pond}(t)$, defined as the fraction of the patch where $h > 1$ mm as a function of time (i.e., where the flow depth h exceeds the model minimum flow threshold of 1 mm).

To describe the tendency for flow to circumvent the patch, flow diversion around it is described with a diversion metric ξ applied to the Lagrangian tracers in the flow. The diversion metric is defined as the fraction of tracers that are initialized directly upslope of the vegetation patch and circumvent it – that is, tracers that reach positions downslope of the patch without passing through it during their trajectory. The ξ is anticipated to increase with increasing resistance contrast between vegetation and bare soil area, and thus with increasing p and ϕ_V.

Table 3: Summary of patch infiltration dynamics for the resource-shedding ($p > K_V$) and resource-capturing ($p < K_V$) cases, separated into rainfall and recession periods. The table indicates whether the patch infiltration fraction (IF_V) is greater or less than one, and how vegetative resistance influences the patch infiltration fraction (ΔIF_V).

	Rainfall period ($t < t_R$)	Recession period ($t > t_R$)
Resource shedding $p > K_V$	Patch generates runoff: $IF_V^{rain} < 1$ Soil permeability limits infiltration into patch: $\Delta IF_V^{rain} = 0$	Net run-on to patch: $IF_V^{rec} < 1$ Roughness slows outflow from patch, prolonging the ponding duration: $\Delta IF_V^{rec} > 0$
Resource capturing $p < K_V$	Net run-on to patch: $IF_V^{rain} > 1$ Vegetative resistance slows run-on: $IF_V^{rain} < 0$	

2.6 Scenario Inter-Comparison Metrics

Finally, to isolate the effects of surface roughness and permeability, we compared assessment metrics between scenarios. First, to assess how vegetative resistance interacts with soil permeability, we examined the difference in IF_V between paired permeability-only and combined-effects simulations (i.e., paired simulations in which only surface roughness differed):

$$\Delta IF_V = IF_V(\text{combined-effects}) - IF_V(\text{permeability-only}), \tag{11}$$

such that $\Delta IF_V > 0$ if vegetative resistance *increases* infiltration in the patch. The difference between combined-effects and resistance-only scenarios is not presented because $K_V = 0.5$ cm/hr in roughness-only scenarios, so that infiltration into the vegetation patch is very small in these scenarios. As a result, the roughness-only scenario does not provide a useful reference point for evaluating the influence of vegetative resistance on infiltration outcomes. In this scenario, roughness primarily influences flow timing, by slowing or delaying runoff—rather than altering infiltration outcomes.

Then, to assess whether K_V influences the runoff diversion around the patch, we computed the difference in ξ between paired roughness-only and combined-effects simulations, in which all parameters were equal except for K_V:

$$\Delta\xi = \xi(\text{combined-effects}) - \xi(\text{roughness-only}). \tag{12}$$

Thus, $\Delta\xi < 0$ indicates that soil permeability in the vegetation patch reduces flow diversion relative to the roughness-only scenario. The difference between combined-effects and resistance-only scenarios is not included because the flow is approximately 1-dimensional in the permeability-only simulations (i.e., $\xi \approx 0$).

3 Results

The simulated runoff and infiltration patterns vary between scenarios, with the differences modulated by rainfall intensity p, vegetation soil permeability K_V, and surface roughness. Throughout the results, a case where the vegetated patch is resource-shedding (with $p > K_V$) is compared with one where the patch is resource-capturing (with $p < K_V$). The diversion parameter ξ is then analyzed across hydrological outcomes to assess the significance of the distortion of the flow paths for these outcomes.

Figure 1 displays the maximum flow depth $h(t_R)$ and cumulative infiltration I. Flow depth is shown in blue shading on the inclined planes and infiltration is shown below in green on the horizontal planes. The top row presents results from a resource-shedding case with $p > K_V$, while the second row presents a resource-capturing case with $p < K_V$. The columns (A-C) present the different modeled scenarios of roughness only (A), permeability only (B), and combined (C).

In the roughness-only cases (panels 1A and 2A), vegetative resistance promotes greater maximum flow depths, but cumulative infiltration is largely unaffected because of the limited soil infiltration capacity. Thus, infiltration is almost identical in the vegetation patch and surrounding bare soil.

In the permeability-only cases (see panels 1B and 2B), greater soil permeability in the vegetation enhances infiltration. In the resource-shedding case (panel 1B), $h(t_R)$ is indistinguishable between surface types because both surface types generate runoff. In the resource-capturing case (panel 2B), run-on to the vegetation is supplied by runoff from upslope, and the maximum depth $h(t_R)$ and cumulative infiltration I both decrease with distance from the upslope boundary of the patch boundary.

Finally, in the combined-effects scenarios, the model predictions are distinct between resource-shedding (panel 1C) and resource-capturing cases (panel 2C). In both cases, vegetative resistance promotes greater maximum flow depths, and greater soil permeability in the vegetation enhances infiltration. In the resource-shedding case, the combination of roughness and permeability enhances I_V compared to the other scenarios. This is because roughness increases the duration of ponding in the vegetation patch during the recession period, particularly towards the downslope boundary of the patch. In the resource-capturing case, by contrast, greater vegetative resistance promotes deeper flows towards the upslope boundary, which decrease with distance downslope as runoff infiltrates. Vegetative resistance thus accentuates the upslope-downslope gradient in patch infiltration compared to the permeability-only scenario (compare panels 2B and 2C).

The inundated fraction F_{pond} in row 3 of Figure 1 illustrates how the infiltration dynamics differ between the three scenarios, for the resource-shedding and resource-capturing cases. Comparison of the combined-effects and permeability-only scenarios provides insight into how roughness further influences infiltration, given the context of higher permeability in vegetation areas. In the resource-shedding case (panel 3A), $F_{pond} = 1$ during the rainfall because $p > K_V$ in all scenarios. When the rain ends, however, resistance to the flow slows the outflow of runoff from the patch in the roughness-only and combined-effects scenarios, but not the permeability-only scenario (compare blue and orange curves in panel 3A). Thus, greater resistance provides a longer time period over which ponded water can infiltrate into the patch, increasing the patch cumulative infiltration (compare panels 1B and 1C).

In the resource-capturing cases, F_{pond} increases more slowly in the combined-effects scenario than the permeability-only scenario during the rainfall, and decreases more slowly in the recession period (panel 3B). By slowing run-on from the upslope boundary, vegetative resistance promotes greater infiltration towards the upslope boundary (compare panels 2B and 2C). Note that $F_{pond} = 1$ during the rainfall in the roughness-only scenario (green line) because $p > K_B$.

Finally, row 4 shows the hillslope hydrographs q_L for each scenario under the resource-shedding case (panel 4A) and resource-capturing case (panel 4B). Despite the differences in the distribution of infiltration between the scenarios, the hydrographs are almost identical. The only difference is the faster rising and recession times in the permeability-only scenario, showing the effect of vegetative resistance at the hillslope scale.

To summarize, in the resource-shedding case, infiltration is enhanced in the combined-effects scenario because vegetative resistance prolongs the duration of water ponding on the

surface thereby increasing the time window for infiltration. In the resource-capturing case, by contrast, vegetative resistance impedes run-on from upslope, enhancing I towards the upslope boundary of the patch and reducing it toward the downslope boundary of the patch.

The relation between cumulative patch infiltration, I_V, and $p - K_V$ is shown in Figure 2, row 1. For a given K_V (see marker shapes), I_V either increases (see $K_V = 10$ cm/hr) or changes minimally (see $K_V = 0.5$ and 2 cm/hr) as a function of $p - K_V$. The sensitivity to rainfall intensity is high in cases with $K_V = 10$ cm/hr (circles markers) because infiltration is limited by the presence of ponded water at the surface ($p < K_V$), so increasing p increases the water available for infiltration. In cases with $p \geq K_V$, by contrast, I_V exhibits minimal sensitivity to $p - K_V$ because patch infiltration is limited by the soil infiltration capacity. In these cases, I_V increases as a function of $p - K_V$ because the recession period – and thus the duration of ponding in the vegetation – is prolonged by increasing runoff generation upslope of the patch.

The patch infiltration fraction IF_V decreases nearly monotonically with increasing $p - K_V$ (see Figure 2, row 2), because infiltration in the patch increases more slowly than the rainfall depth (i.e., the denominator in $IF_V = I_V/d_R$ increases faster than the numerator as $p - K_V$ increases). The vegetation is a net runoff sink in cases with $p - K_V < 1$, and generates runoff in cases with $p - K_V > 1$. The transition between resource shedding and capturing behaviors occurs for $p - K_V > 1$ cm/hr because of infiltration that occurs from run-on to the patch during the recession period (after the rainfall, the vegetation patch captures water ponded within the patch and in the upslope bare soil area). In general, the transition between source and sink behaviors can occur for larger values of $p - K_V$, depending on the range of environmental conditions. Within the full simulation ensemble, it varies from 1 to 4 cm/hr (see SI Figure S2). The threshold likely also varies with variables held constant in these simulations, including the rainfall duration, vegetation patch size, and domain geometry (e.g., the upslope area contributing runoff).

3.1 Isolating Roughness Effects on Patch Infiltration

Figure 3 presents the patch infiltration fraction IF_V (row 1) and how vegetative resistance influences it, ΔIF_V (row 2), as a function of the rainfall excess, $p - K_V$. Positive values of ΔIF_V indicate that vegetative resistance increases patch infiltration. The figure columns present the full simulation (column A), rainfall (column B), and recession periods (column C). In panel 1B, IF_V^{rain} decreases monotonically as the proportion of rainfall absorbed by the patch decreases. In panel 1C, $IF_V^{rec} < 1$, indicating that run-on inputs never exceed the total rainfall depth, and is greatest when $p - K_V = -3$ cm/hr. Panel 1A is repeated from Figure 2 for comparison.

The effect of vegetation resistance on patch infiltration varies between the rainfall and recession periods. During the rainfall period, vegetative resistance slows run-on from the upslope bare soil area. When $p - K_V < 0$, this reduces infiltration into the patch (see negative ΔIF_V in panel 2B). For $p - K_V \geq 0$, there is no effect because the patch remains uniformly inundated ($F_{pond} = 1$) throughout the rainfall. During the recession period, vegetative resistance increases infiltration by extending the ponding duration in the patch (see $\Delta IF_V > 0$ for all values of $p - K_V$ in panel 2C) and increases with stem density ϕ_V (indicated by marker size).

Considering the complete simulation period, the sign change in ΔIF_V reflects the contrasting effects of the rainfall versus recession-period dynamics ($\Delta IF_V^{rain} \leq 0$ in panel 2B and $\Delta IF_V^{rec} \geq 0$ in panel 2C). Combining the rainfall and recession periods, the spatial association between surface roughness and permeability can increase the patch infiltration fraction by up to 25% and decrease it by up to 15% in the modeled scenarios, depending on $p - K_V$ (see

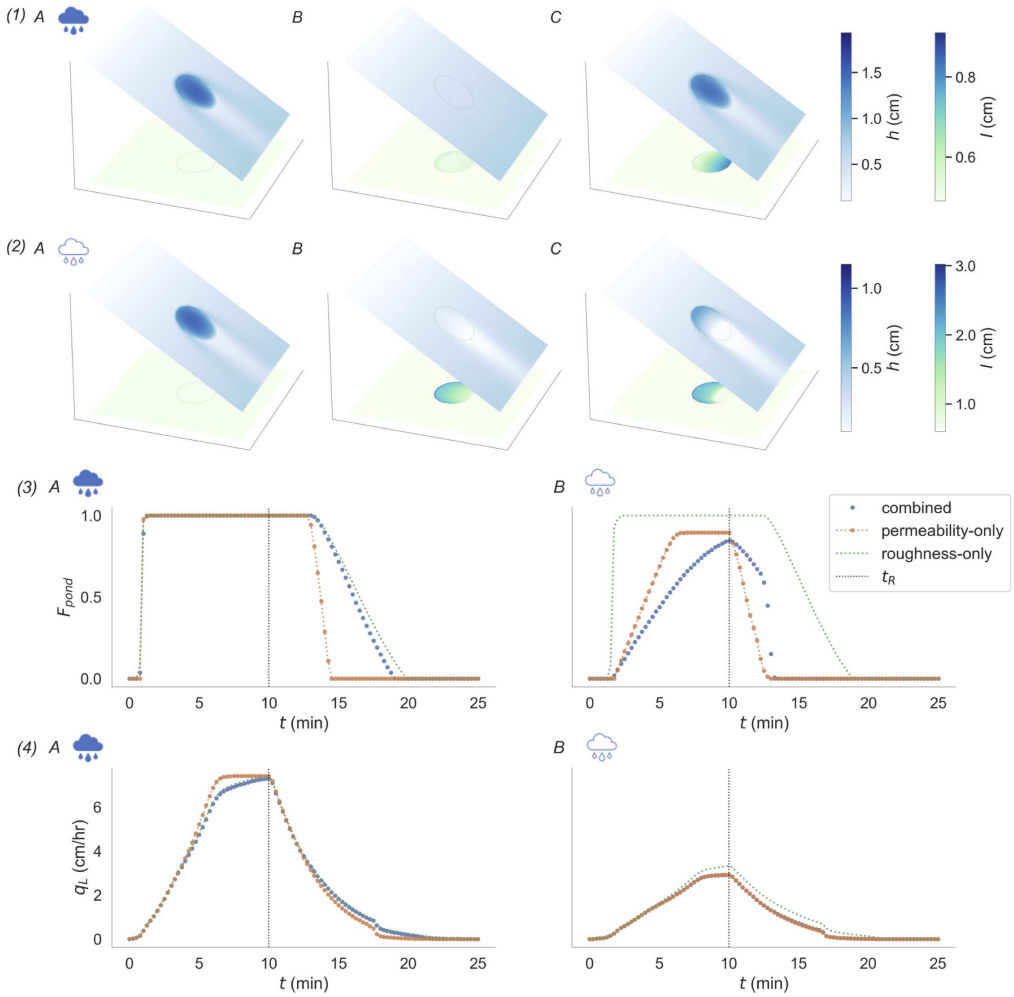

Figure 1: Rows 1 and 2 compare the model simulation results between scenarios for two rainfall cases: a 'resource-shedding' case with rainfall intensity $p = 8$ cm/hr, vegetation saturated hydraulic conductivity $K_V = 2$ cm/hr, and stem density $\phi_V = 0.2$, and a 'resource-capturing' case with $p = 4$ cm/hr, $K_V = 10$ cm/hr, and $\phi_V = 0.2$ (all other parameters are listed in Table 1). Blue shading on the inclined planes shows the maximum flow depth $h(t_R)$, and blue-green shading on the horizontal planes shows the cumulative infiltration. From left to right, columns indicate (A) roughness-only, (B) permeability-only, and (C) combined-effects scenarios. Rows 3 and 4 show the inundated fraction F_{pond} and hillslope hydrographs q_L, respectively, for the resource-shedding (A) and resource-capturing (B) scenarios. Cloud markers connect the rainfall cases between rows 1-2 and 3-4, with the transparent cloud indicating the resource-conserving case.

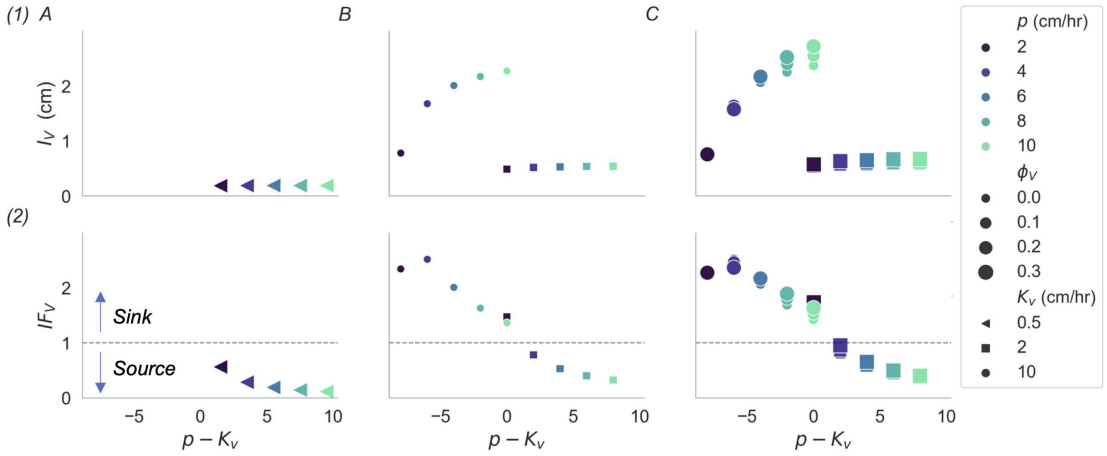

Figure 2: Summary plots showing the patch cumulative infiltration I_V (row 1) and patch infiltration fraction IF_V (row 2), plotted as a function of the rainfall intensity p minus the vegetation saturated hydraulic conductivity K_V. Columns show the three simulation scenarios: (A) 'roughness-only' – with spatially-uniform soil permeability ($K_B = 0.5$ cm/hr), (B) 'permeability-only' – with spatially-uniform surface roughness ($\phi_V = 0$), and (C) 'combined-effects', with spatial variation in both roughness and soil permeability ($K_V > K_B$ and $\phi_V > 0$). Marker shapes indicate K_V, marker sizes indicate the vegetation stem density ϕ_V, and marker colors indicate p. Marker shapes differ between panels because scenarios are distinguished by K_V and roughness parameterizations (see Section 2.2). Source and sink arrows in panel 2A indicate the transition between resource-shedding and resource-conserving cases, respectively.

panel 2A). ΔIF_V changes sign from negative to positive around $p - K_V = -4$ cm/hr. The threshold $p - K_V$ for which ΔIF_V changes sign depends on K_V, and ranges from -9 to -3 cm/hr across the full simulation ensemble (see SI Figure S3). Other parameters, such as the patch radius, bare soil permeability, and storm duration t_R, are also likely to influence the value of this threshold, but were not explored in these simulations.

The signature of vegetative resistance is also visible in spatial patterns of cumulative infiltration. These patterns also differ between the rainfall and recession periods (see Figure 3, rows 3 and 4, which illustrates for the same resource-shedding and resource-capturing simulations featured in Figure 1). In the resource-shedding case, infiltration is enhanced towards the downslope patch boundary (see panel 3A). This is because vegetative resistance slows the flow of runoff out of the patch during the recession period, prolonging the ponding duration most towards the downslope patch boundary where runoff exits the patch (panel 3C). Vegetative resistance has no effect on infiltration during the storm (panel 3B).

In the resource-capturing case, by contrast, vegetative resistance promotes infiltration towards the upslope patch boundary and reduces it towards the downslope boundary (see Figure 3, panel 4A). During the rainfall period (panel 4B), vegetative resistance slows run-on into the patch and reduces the distance run-on travels. Then, during the recession period, vegetative resistance slows runoff within the patch, promoting infiltration towards the upslope boundary by increasing the ponding duration there (see panel 4C). Combining rainfall and recession periods, cumulative infiltration is enhanced towards the upslope boundary and reduced towards the downslope boundary, creating the spatial contrast in panel 4A.

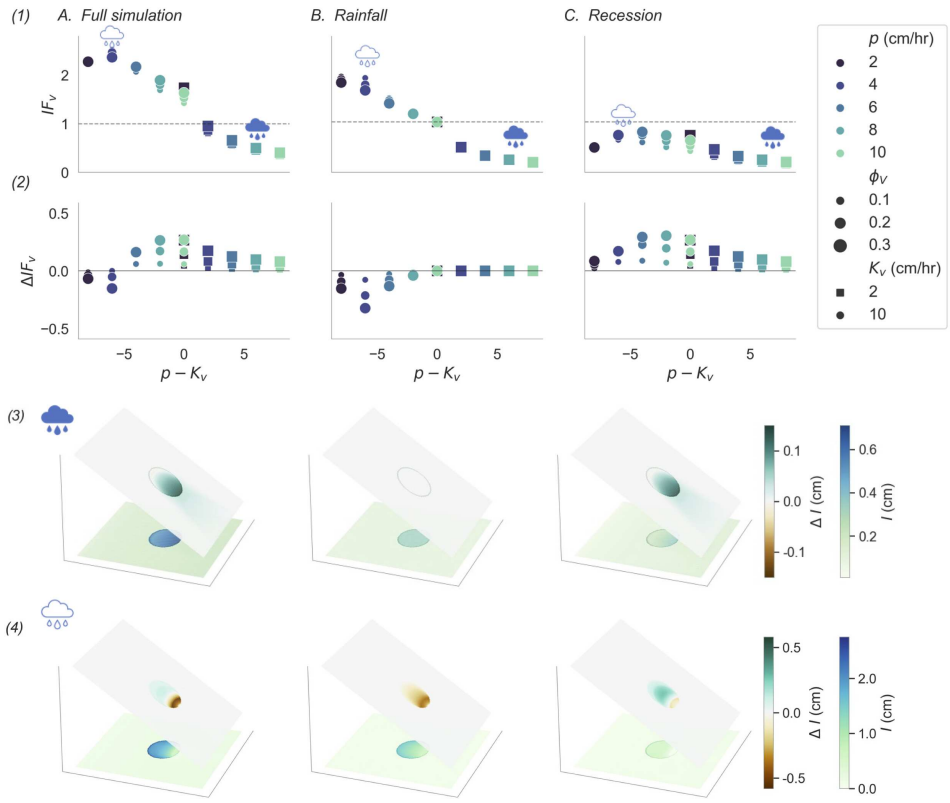

Figure 3: Row 1 shows the combined-effects patch infiltration fraction IF_V for the full simulation period (column A), rainfall period (column B) and recession period (column C). Row 2 shows ΔIF_V – the difference in IF_V between paired combined-effects and permeability-only simulations. $\Delta IF_V > 0$ indicates greater IF_V in the combined-effects scenario (i.e., vegetative resistance promotes infiltration). Marker colors indicate p, shapes indicate K_V, and sizes indicate the vegetation stem density ϕ_V. Rows 3 and 4 illustrate the spatial patterns of cumulative infiltration for the same cases as in Figure 1: a 'resource-shedding' case with $p = 8$ cm/hr and $K_V = 2$ cm/hr (row 3), and a 'resource-capturing' case with $p = 4$ cm/hr and $K_V = 10$ cm/hr (row 4). The cumulative infiltration I is projected onto the horizontal planes (blue-green shading), and ΔI_V is shown on the inclined planes (brown-green shading). Other parameters are $\phi_V = 0.2$, patch radius $r = 5$ m, storm duration $t_R = 10$ min, and slope gradient $S_o = 1\%$. Cloud markers connect the rainfall cases between rows 1-2 and rows 3-4, with the transparent cloud indicating the resource-conserving case.

3.2 Diversion

To illustrate the flow diversion, rows 1 and 2 in Figure 4 show the paths of 500 tracers for the same cases as Figures 2 and 3. Diversion around the patch is apparent for the roughness-only and combined-effects scenarios (columns A and C), while in the permeability-only cases (column B), flow is almost entirely 1-dimensional and not diverted. In panel 2B, high permeability in the vegetation patch causes slight flow convergence downslope of the patch by lowering the flow depth, attracting water in from the surrounding bare soil area. This attraction has the opposite effect of flow resistance, promoting flow convergence into the patch instead of divergence around it.

While the patch infiltration varies as a function of $p - K_V$, the flow diversion ξ depends more closely on p (see Figure 4, row 3, which shows ξ as a function of p for each scenario). In the roughness-only and combined-effects scenarios (columns A and C), the flow diversion increases with p and stem density ϕ_V (see marker size), showing minimal sensitivity to K_V (marker color). The flow diversion is zero in the permeability-only scenario (column B).

For a given p and ϕ_V, the flow diversion decreases with increasing K_V; however, the effect is minor. The difference in ξ between paired combined-effects and roughness-only simulations, $\Delta\xi$, is negative in all cases (see grey-shaded markers in Figure 4, panel 1C). The most extreme $\Delta\xi$ is just -2%, with $p = 10$ cm/hr, $K_V = 15$ cm/hr, and $\phi_V = 0.3$ cm/hr (see SI Figure S4).

The simulation results using Manning's equation are presented in SI Figures S5-S7. The details of the simulation results differ between resistance formulations; however, the results are qualitatively similar.

4 Discussion

Measuring in-situ the shallow surface flows involved in such problems is difficult, and a comprehensive understanding of the factors that influence redistribution is still evolving [23]. Vegetation influences rainfall runoff through a plethora of processes other than permeability contrasts, including interception losses [34, 63], changes in microtopography [6], surface-tension driven flow processes [21], changes in surface roughness [27, 49], stemflow, rock outcrops, surface depression storage, antecedent soil moisture and raindrop impacts [known to increase flow resistance, particularly in bare soil areas without canopy cover protection, 52].

The model results presented here are not intended to quantify which of those aforementioned processes dominate. Rather, they seek to delineate the plausible conditions under which run-around occurs, without resorting to alternative explanations such as microtopography, surface tension, or interception loss contrasts, among others. The study presents a defined model experiment to investigate the relations between flow, permeability and roughness for an isolated patch. The advantages of this approach are that the results can be clearly interpreted in terms of soil-vegetation contrast. Other factors known to influence surface runoff are omitted to preserve such interpretability.

Binarization of the landscape into vegetation and bare soil imposes artificially sharp boundaries, which may be inappropriate in some cases. For example, in many dryland environments, the influence of root macropores extends beyond the plant canopy into unvegetated soils, increasing the soil infiltrability and blurring the distinction between surface types [20]. In neglecting these and other ecohydrologically-important factors, the study findings are constrained to delineating the roles of spatially-correlated roughness and permeability in influencing surface runoff.

The findings here suggest that the influence of vegetative resistance alone on $h(t_R)$ and I dynamically differs between rainfall and recession periods, as illustrated by two limiting cases: (1) a 'resource capture' limit, in which all surface runoff generated in the bare soil area

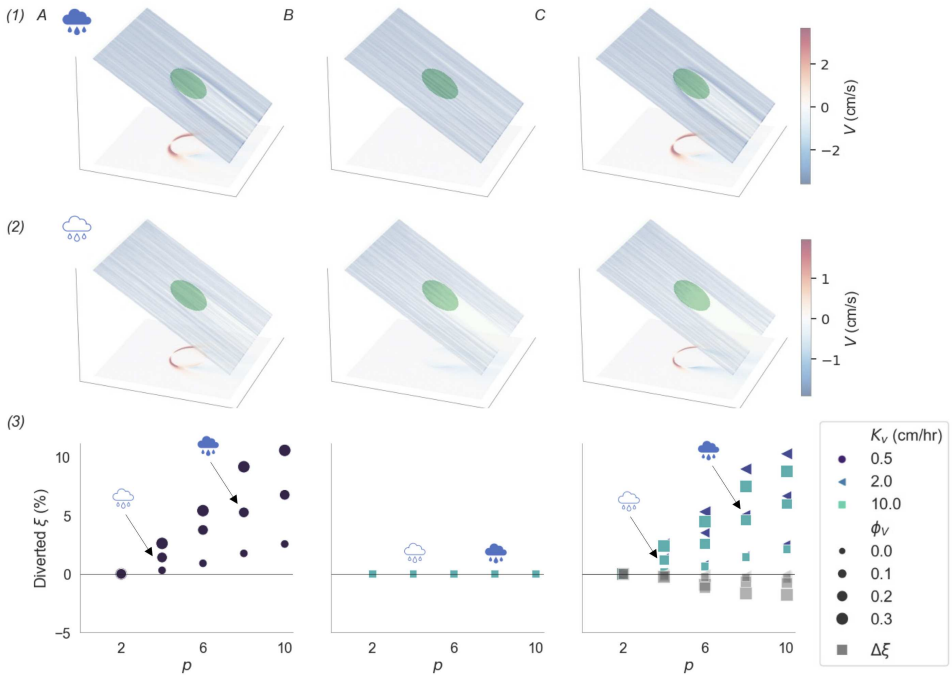

Figure 4: Rows 1 and 2 illustrate the flow diversion for the same cases as in Figure 1: a 'resource-shedding' case with rainfall intensity $p = 8$ cm/hr and saturated hydraulic conductivity $K_V = 2$ cm/hr (row 1), and a 'resource-capturing' cases with $p = 4$ cm/hr and $K_V = 10$ cm/hr (row 2). Columns indicate the three simulation scenarios: (A) roughness-only, (B) permeability-only, and (C) combined-effects scenarios. Row 3 shows the tracer diversion percent ξ for each scenario. Grey markers in panel 3C show $\Delta\xi$, the diversion difference between roughness-only and combined-effects scenarios, with negative values indicating that increasing the vegetation saturated hydraulic conductivity, K_V, reduces diversion. Marker colors indicate K_V, and marker size indicates the vegetation stem density ϕ_V. Marker shapes differ between panels because scenarios are distinguished by K_V and roughness parameterizations (see Section 2.2).

flows into and infiltrates within the vegetation patch, and (2) a 'resource shedding' limit, in which rainfall intensity exceeds the patch infiltration capacity, resulting in water and other resources lost from the hillslope. In the resource-capture limit, greater vegetative resistance reduces cumulative infiltration in vegetation patches: roughness slows run-on, reducing the fraction of vegetation that receives run-on inputs from upslope of the vegetation. In resource-shedding cases, by contrast, where rainfall intensity exceeds the infiltration capacity of the soil, greater roughness enhances the cumulative infiltration within vegetation. In these cases, roughness increases the depth of water ponded in the vegetation, and following the cessation of rain provides a longer 'window of opportunity' for water to infiltrate. Positive ΔIF_V in the resource-shedding limit reflects recession-period dynamics, whereas negative ΔIF_V in the resource-capturing limit reflects transient dynamics during the rainfall. Between these limits, the effect of vegetative resistance changes in sign from increasing infiltration (resource-shedding) to reducing it (resource-capturing).

The simulation ensemble did not include variation in all variables likely to influence the patch infiltration fraction (IF_V), nor all variables likely to modulate how vegetative resistance influences it (ΔIF_V). The directional effect of some variables may be predicted by considering the storm and recession period dynamics separately. The potential sensitivity of IF_V is discussed below for two such variables: storm duration t_R and patch radius r.

Due to the short duration of the simulated rainfall, the flow was not in steady-state for a significant portion of the simulations. In resource-shedding cases ($p > K_V$), positive ΔIF_V reflects transient, recession-period dynamics, so ΔIF_V is expected to decrease with increasing rainfall duration. Similarly, in resource-capturing cases, negative ΔIF_V reflects transient dynamics associated with the wetting front's advancement from the upslope boundary. In this case, increasing the rainfall duration will increase ΔIF_V (less negative). In both cases, ΔIF_V approaches zero as the storm duration increases. This is because, during prolonged rainfall, the patch inundated fraction F_{pond} is determined by the balance between upslope runoff supply and patch infiltration capacity. In this case, the effects of vegetative resistance on infiltration are limited to transient flow periods.

Increasing the patch radius creates a larger area over which the vegetation may influence the flow. In the low $p - K_V$ limit, vegetative resistance would slow the wetting front over a larger area, which may decrease its impact on IF_V (i.e., less negative ΔIF_V). This is because the additional area contributes more to the denominator of IF_V than to the difference in infiltration between scenarios, particularly if the wetting front does not reach the downslope edge of the patch. In the high $p - K_V$ limit, increasing patch radius may increase the time required for ponded water to flow out of the vegetation, increasing ΔIF_V.

While the study findings were robust to the choice of resistance formulation (compare Figures 2-4 to SI Figures S5-S7, showing the results generated using Manning's equation), these resistance formulations both omit processes known to influence flow resistance, including litter cover, raindrop impact, and surface tension [21]. Flow resistance also depends on flow regime, which may be laminar or turbulent or a mixture of the two (transitional) [48, 62]. Moreover, the resistance formulation does not account for surface tension [21]. The choice of roughness scheme and its parameterization influences the model predictions, but is unlikely to change the study conclusions, provided the models central features – greater resistance and soil permeability in vegetation – are retained.

While vegetative resistance diverts some flow around the vegetation, this effect did not reduce the cumulative infiltration in the vegetation compared to a case where only permeability differs with the surrounding bare soil. However, the implications of the 'run-around' behavior may differ between cumulative infiltration and sediment, solutes, and seed transport. For materials transported by runoff, the total volume flux through the patch may be most relevant to the trapping potential of the vegetation (i.e., the potential for materials to be

trapped by vegetation stems and litter and remain in the patch). In such applications, the run-around effect may contribute to resource-shedding behavior; however, the effect is likely small (<12% in the simulation domain considered here). Future studies could explore the impact of flow diversion around patches on deposition of materials within vegetated sites.

The results show that hydrologic and hydraulic processes are weakly coupled in the simulated domain: flow diversion around the patch (a hydraulic effect) does not reduce infiltration in the patch (a hydrologic outcome). Similarly, increasing soil permeability in the vegetation (a hydrologic boundary condition) has a minimal effect on the flow diversion. While increasing patch roughness is associated with greater flow diversion ξ, the influence of patch roughness on ΔIF_V is more nuanced. Depending on the rainfall and surface conditions, roughness can increase infiltration by prolonging ponding during the recession period, or reduce it by slowing run-on during rainfall.

Discussions of dryland source-sink dynamics typically focus on the central role of soil permeability in facilitating the redistribution of resources between bare soil and vegetation [40, 51], as do landscape indicators such as the Flowlength metric [4, 47]. Similarly, in modeling studies targeting runoff run-on processes or source-sink connectivity, characterization of runoff run-on processes typically focuses on spatial variation in infiltration rates (a hydrologic property), considering vegetation patches as runoff sinks [15, 35, 57]. The study results suggest that the errors arising from this simplification are likely small ($< 10\%$), such that omitting spatial contrasts in surface roughness is plausible in a first order analysis.

5 Conclusions

In a series of hillslope runoff simulations using a 2D Saint Venant Equation model – paired with particle tracing to identify flow paths – the effect of vegetative resistance on runoff and infiltration patterns varied depending on storm and soil conditions. Vegetative resistance functions to decrease infiltration during the rainfall and increase it during the recession period. The net influence on the patch infiltration fraction, IF_V, depends on competing dynamics during the rainfall and recession periods, which in turn depends on the rainfall intensity, soil permeability, and stem density. In most cases, greater surface roughness in the vegetation patch than in the surrounding area slows runoff and increases its residence time, promoting infiltration in the patch. The exception is in cases where the infiltration capacity of the vegetation exceeds the rainfall intensity (i.e., $p < K_V$). For the modeled scenarios, the spatial association between surface roughness and permeability may increase the patch infiltration fraction by as much as 25% and decrease it by as much as 15%, with the sign depending on the rainfall excess, $p - K_V$. Greater resistance within vegetated sites also contributes to a 'run around' effect, whereby flow is diverted around the vegetation patch; however, the effect does not reduce the cumulative infiltration in the patch.

Acknowledgements

OC acknowledges funding from the National Science Foundation (NSF) grant number EAR-PF-1952651; and GK acknowledges support from NSF-AGS-2028644, and the U.S. Department of Energy (DE-SC0022072).

Data availability

This manuscript relied only on model output generated by the authors during the course of the study. Version 1.09 of FullSWOF_2D used for the model simulations is available at DOI 10.21105/joss.00448 via CeCILL and developed openly at https://www.idpoisson.fr/fullswof/. The model simulation results used in the study are available at Open Science Foundation at https://osf.io/rn63v/

Author Contributions

OC: Conceptualization, Methodology, Software, Writing—Original Draft, Writing—Review & Editing, Visualization.
GK: Conceptualization, Methodology, Writing—Original Draft, Writing—Review & Editing.
ST: Writing—Review & Editing.

References

[1] D. K. Adams and A. C. Comrie. The north american monsoon. *Bulletin of the American Meteorological Society*, 78(10):2197–2214, 1997.

[2] E. Arnau-Rosalén, A. Calvo-Cases, C. Boix-Fayos, H. Lavee, and P. Sarah. Analysis of soil surface component patterns affecting runoff generation. an example of methods applied to mediterranean hillslopes in alicante (spain). *Geomorphology*, 101(4):595–606, 2008.

[3] S. Assouline. Rainfall-induced soil surface sealing: A critical review of observations, conceptual models, and solutions. *Vadose Zone Journal*, 3(2):570–591, 2004.

[4] S. Bautista, A. G. Mayor, J. Bourakhouadar, and J. Bellot. Plant spatial pattern predicts hillslope runoff and erosion in a semiarid mediterranean landscape. *Ecosystems*, 10(6): 987–998, 2007.

[5] J. Belnap. The potential roles of biological soil crusts in dryland hydrologic cycles. *Hydrological Processes: An International Journal*, 20(15):3159–3178, 2006.

[6] G. Bergkamp. A hierarchical view of the interactions of runoff and infiltration with vegetation and microtopography in semiarid shrublands. *Catena*, 33(3-4):201–220, 1998.

[7] E. Bochet, J. Poesen, and J. L. Rubio. Mound development as an interaction of individual plants with soil, water erosion and sedimentation processes on slopes. *Earth Surface Processes and Landforms: The Journal of the British Geomorphological Research Group*, 25(8):847–867, 2000.

[8] W. Brutsaert. *Hydrology: an introduction*. Cambridge university press, 2005.

[9] L. Cea, C. Legout, F. Darboux, M. Esteves, and G. Nord. Experimental validation of a 2d overland flow model using high resolution water depth and velocity data. *Journal of hydrology*, 513:142–153, 2014.

[10] N.-S. Cheng and H. T. Nguyen. Hydraulic radius for evaluating resistance induced by simulated emergent vegetation in open-channel flows. *Journal of hydraulic engineering*, 137(9):995–1004, 2011.

[11] V. Chow. Open channel flow. macgraw-hill book co. *Inc.: New York*, 1959.

[12] O. Crompton, A. Sytsma, and S. Thompson. Emulation of the saint venant equations enables rapid and accurate predictions of infiltration and overland flow velocity on spatially heterogeneous surfaces. *Water Resources Research*, 55(8):7108–7129, 2019.

[13] O. Crompton, G. G. Katul, and S. Thompson. Resistance formulations in shallow overland flow along a hillslope covered with patchy vegetation. *Water Resources Research*, 56(5):e2020WR027194, 2020.

[14] O. Crompton, G. Katul, D. Lapides, and S. Thompson. Hydrologic connectivity and patch-to-hillslope scale relations in dryland ecosystems. *Geophysical Research Letters*, 50(10):e2022GL101801, 2023. doi: https://doi.org/10.1029/2022GL101801. URL https://agupubs.onlinelibrary.wiley.com/doi/abs/10.1029/2022GL101801. e2022GL101801 2022GL101801.

[15] O. Crompton, G. Katul, D. A. Lapides, and S. E. Thompson. Bridging structural and functional hydrological connectivity in dryland ecosystems. *CATENA*, 231:107322, 2023.

[16] O. Crompton, G. Katul, and S. E. Thompson. Relating flow resistance to equivalent roughness. *Advances in Water Resources*, 195:104855, 2025.

[17] O. Crompton, G. Katul, and S. E. Thompson. Uniting surface properties with hydrodynamic roughness in shallow overland flow models. *Water Resources Research*, 61(1): e2024WR037176, 2025.

[18] O. Delestre, C. Lucas, P.-A. Ksinant, F. Darboux, C. Laguerre, T.-N.-T. Vo, F. James, and S. Cordier. Swashes: a compilation of shallow water analytic solutions for hydraulic and environmental studies. *International Journal for Numerical Methods in Fluids*, 72 (3):269–300, 2013.

[19] O. Delestre, S. Cordier, F. Darboux, M. Du, F. James, C. Laguerre, C. Lucas, and O. Planchon. Fullswof: A software for overland flow simulation. *Advances in Hydroinformatics: SIMHYDRO 2012–New Frontiers of Simulation*, pages 221–231, 2014.

[20] D. Dunkerley. Hydrologic effects of dryland shrubs: defining the spatial extent of modified soil water uptake rates at an australian desert site. *Journal of Arid Environments*, 45 (2):159–172, 2000.

[21] D. Dunkerley. Surface tension and friction coefficients in shallow, laminar overland flows through organic litter. *Earth Surface Processes and Landforms: The Journal of the British Geomorphological Research Group*, 27(1):45–58, 2002.

[22] D. L. Dunkerley. Infiltration rates and soil moisture in a groved mulga community near alice springs, arid central australia: evidence for complex internal rainwater redistribution in a runoff–runon landscape. *Journal of Arid Environments*, 51(2):199–219, 2002.

[23] D. L. Dunkerley. Determining friction coefficients for interrill flows: the significance of flow filaments and backwater effects. *Earth Surface Processes and Landforms: The Journal of the British Geomorphological Research Group*, 28(5):475–491, 2003.

[24] D. L. Dunkerley and K. J. Brown. Banded vegetation near broken hill, australia: significance of surface roughness and soil physical properties. *Catena*, 37(1-2):75–88, 1999.

[25] T. Dunne and W. E. Dietrich. Experimental study of horton overland flow on tropical hillslopes. *Soil conditions, infiltration and frequency of runoff*, 2:40–80, 1980.

[26] T. Dunne, W. Zhang, and B. F. Aubry. Effects of rainfall, vegetation, and microtopography on infiltration and runoff. *Water Resources Research*, 27(9):2271–2285, 1991.

[27] P. Garcia-Estringana, N. Alonso-Blázquez, M. Marques, R. Bienes, and J. Alegre. Direct and indirect effects of mediterranean vegetation on runoff and soil loss. *European Journal of Soil Science*, 61(2):174–185, 2010.

[28] M. Hernandez, S. N. Miller, D. C. Goodrich, B. F. Goff, W. G. Kepner, C. M. Edmonds, and K. Bruce Jones. Modeling runoff response to land cover and rainfall spatial variability in semi-arid watersheds. In *Monitoring Ecological Condition in the Western United States*, pages 285–298. Springer, 2000.

[29] A. Imeson and H. Prinsen. Vegetation patterns as biological indicators for identifying runoff and sediment source and sink areas for semi-arid landscapes in spain. *Agriculture, ecosystems & environment*, 104(2):333–342, 2004.

[30] C. James, A. Birkhead, A. Jordanova, and J. O'sullivan. Flow resistance of emergent vegetation. *Journal of Hydraulic Research*, 42(4):390–398, 2004.

[31] P. Y. Julien, B. Saghafian, and F. L. Ogden. Raster-based hydrologic modeling of spatially-varied surface runoff 1. *JAWRA Journal of the American Water Resources Association*, 31(3):523–536, 1995.

[32] J. Ludwig, D. Tongway, K. Hodgkinson, D. Freudenberger, and J. Noble. *Landscape ecology, function and management: principles from Australia's rangelands*. Csiro Publishing, 1996.

[33] F. T. Maestre, R. Salguero-Gomez, and J. L. Quero. It is getting hotter in here: determining and projecting the impacts of global environmental change on drylands, 2012.

[34] P. N. Magliano, J. I. Whitworth-Hulse, and G. Baldi. Interception, throughfall and stemflow partition in drylands: Global synthesis and meta-analysis. *Journal of Hydrology*, 568:638–645, 2019.

[35] A. G. Mayor, S. Bautista, F. Rodriguez, and S. Kéfi. Connectivity-mediated ecohydrological feedbacks and regime shifts in drylands. *Ecosystems*, 22(7):1497–1511, 2019.

[36] M. Melis, D. Poggi, O. D. Fasanella, Giovanni, S. Cordero, and G. G. Katul. Resistance to flow on a sloping channel covered by dense vegetation following a dam break. *Water Resources Research*, 55(2):1040–1058, 2019.

[37] K. Michaelides, D. Lister, J. Wainwright, and A. J. Parsons. Vegetation controls on small-scale runoff and erosion dynamics in a degrading dryland environment. *Hydrological Processes: An International Journal*, 23(11):1617–1630, 2009.

[38] M. Moreno-De-Las-Heras, L. Merino-Martín, P. M. Saco, T. Espigares, F. Gallart, and J. M. Nicolau. Structural and functional control of surface-patch to hillslope runoff and sediment connectivity in mediterranean dry reclaimed slope systems. *Hydrology and Earth System Sciences*, 24(5):2855–2872, 2020.

[39] C. Mügler, O. Planchon, J. Patin, S. Weill, N. Silvera, P. Richard, and E. Mouche. Comparison of roughness models to simulate overland flow and tracer transport experiments under simulated rainfall at plot scale. *Journal of Hydrology*, 402(1-2):25–40, 2011. doi: 10.1016/j.jhydrol.2011.02.032.

[40] I. Noy-Meir. Structure and function of desert ecosystems. *Israel Journal of Plant Sciences*, 28(1):1–19, 1979.

[41] G. S. Okin, A. J. Parsons, J. Wainwright, J. E. Herrick, B. T. Bestelmeyer, D. C. Peters, and E. L. Fredrickson. Do changes in connectivity explain desertification? *BioScience*, 59(3):237–244, 2009.

[42] G. S. Okin, M. M.-d. l. Heras, P. M. Saco, H. L. Throop, E. R. Vivoni, A. J. Parsons, J. Wainwright, and D. P. Peters. Connectivity in dryland landscapes: shifting concepts of spatial interactions. *Frontiers in Ecology and the Environment*, 13(1):20–27, 2015.

[43] G. G. Penny, K. E. Daniels, and S. E. Thompson. Local properties of patterned vegetation: quantifying endogenous and exogenous effects. *Philosophical Transactions of the Royal Society A: Mathematical, Physical and Engineering Sciences*, 371(2004):20120359, 2013.

[44] V. Polyakov, J. Stone, C. Holifield Collins, M. A. Nearing, G. Paige, J. Buono, and R.-L. Gomez-Pond. Rainfall simulation experiments in the southwestern usa using the walnut gulch rainfall simulator. *Earth System Science Data*, 10(1):19–26, 2018.

[45] J. Puigdefábregas. The role of vegetation patterns in structuring runoff and sediment fluxes in drylands. *Earth Surface Processes and Landforms: The Journal of the British Geomorphological Research Group*, 30(2):133–147, 2005.

[46] J. F. Reynolds, D. M. S. Smith, E. F. Lambin, B. Turner, M. Mortimore, S. P. Batterbury, T. E. Downing, H. Dowlatabadi, R. J. Fernández, J. E. Herrick, et al. Global desertification: building a science for dryland development. *science*, 316(5826):847–851, 2007.

[47] F. Rodríguez, A. G. Mayor, M. Rietkerk, and S. Bautista. A null model for assessing the cover-independent role of bare soil connectivity as indicator of dryland functioning and dynamics. *Ecological Indicators*, 94:512–519, 2018.

[48] J. Roels. Flow resistance in concentrated overland flow on rough slope surfaces. *Earth Surface Processes and Landforms*, 9(6):541–551, 1984.

[49] M. J. Rossi and J. O. Ares. Overland flow from plant patches: Coupled effects of preferential infiltration, surface roughness and depression storage at the semiarid patagonian monte. *Journal of Hydrology*, 533:603–614, 2016.

[50] M. J. Rossi and J. O. Ares. Water fluxes between inter-patches and vegetated mounds in flat semiarid landscapes. *Journal of Hydrology*, 546:219–229, 2017.

[51] W. H. Schlesinger, J. F. Reynolds, G. L. Cunningham, L. F. Huenneke, W. M. Jarrell, R. A. Virginia, and W. G. Whitford. Biological feedbacks in global desertification. *Science*, 247(4946):1043–1048, 1990.

[52] E. Shen, G. Liu, Y. Jia, C. Dan, M. A. Abd Elbasit, C. Liu, J. Gu, and H. Shi. Effects of raindrop impact on the resistance characteristics of sheet flow. *Journal of Hydrology*, 592:125767, 2021.

[53] M. W. Smith, N. J. Cox, and L. J. Bracken. Applying flow resistance equations to overland flows. *Progress in Physical Geography*, 31(4):363–387, 2007.

[54] Y. Tanino and H. M. Nepf. Laboratory investigation of mean drag in a random array of rigid, emergent cylinders. *Journal of Hydraulic Engineering*, 134(1):34–41, 2008.

[55] L. Tatard, O. Planchon, J. Wainwright, G. Nord, D. Favis-Mortlock, N. Silvera, O. Ribolzi, M. Esteves, and C. H. Huang. Measurement and modelling of high-resolution flow-velocity data under simulated rainfall on a low-slope sandy soil. *Journal of Hydrology*, 348(1-2):1–12, 2008.

[56] S. Thompson, G. Katul, A. Konings, and L. Ridolfi. Unsteady overland flow on flat surfaces induced by spatial permeability contrasts. *Advances in water resources*, 34(8): 1049–1058, 2011.

[57] L. Turnbull and J. Wainwright. From structure to function: Understanding shrub encroachment in drylands using hydrological and sediment connectivity. *Ecological indicators*, 98:608–618, 2019.

[58] A. M. Urgeghe, A. G. Mayor, D. Turrión, F. Rodríguez, and S. Bautista. Disentangling the independent effects of vegetation cover and pattern on runoff and sediment yield in dryland systems–uncovering processes through mimicked plant patches. *Journal of Arid Environments*, 193:104585, 2021.

[59] R. Vásquez-Méndez, E. Ventura-Ramos, K. Oleschko, L. Hernández-Sandoval, J.-F. Parrot, and M. A. Nearing. Soil erosion and runoff in different vegetation patches from semiarid central mexico. *Catena*, 80(3):162–169, 2010.

[60] J. Wainwright, A. J. Parsons, and A. D. Abrahams. Plot-scale studies of vegetation, overland flow and erosion interactions: Case studies from arizona and new mexico. *Hydrological Processes*, 14(16-17):2921–2943, 2000.

[61] B. P. Wilcox. Runoff from rangelands: the role of shrubs. *Shrub management. Texas A&M University, College Station, Texas, USA*, 2003.

[62] D. A. Woolhiser, C. Hanson, and A. Kuhlman. Overland flow on rangeland watersheds. *Journal of Hydrology (New Zealand)*, pages 336–356, 1970.

[63] C. B. Zou, G. L. Caterina, R. E. Will, E. Stebler, and D. Turton. Canopy interception for a tallgrass prairie under juniper encroachment. *PLoS One*, 10(11):e0141422, 2015.